ACTA ACUSTICA UNITED WITH ACUSTICA
Vol. 101 (2015) 300 – 316

DOI 10.3813/AAA.918828

Regime Change Thresholds in Recorder-Like Instruments: Influence of the Mouth Pressure Dynamics

Soizic Terrien[1)], Rémi Blandin[1)*], Christophe Vergez[1)], Benoît Fabre[2)]

[1)] LMA, CNRS, UPR 7051, Aix-Marseille Univ, Centrale Marseille, 13402 Marseille Cedex 20, France. terrien@lma.cnrs-mrs.fr

[2)] LAM, Sorbonne Universités, UPMC Univ Paris 06, CNRS, UMR 7190, Institut Jean Le Rond d'Alembert, 11 rue de Lourmel F-75015 Paris, France.

Summary

In the recorder, variation in blowing pressure can produce changes between playing regimes and thus jumps from one note to another. In this paper, such transitions are compared for a recorder played by an experienced player, a person with no playing experience, and an artificial mouth. The experienced player is observed to shift regime change thresholds up to 240% and 292% compared to the artificial mouth and the non musician (respectively), and thus to enlarge the control of nuances and spectrum. The hypothesis that the dynamics (*i.e.* rate of change) of the blowing pressure influences regime change thresholds is tested experimentally using an artificial mouth and numerically through time-domain simulations of a physical model of the instrument. Regime change thresholds are compared for both linearly varying blowing pressure profiles with different slopes and for piecewise linear ramps of the blowing pressure (including a slope change). The results highlight a strong dependence of thresholds on the blowing pressure dynamics. A phenomenological model of the register change that predicts regime change as a function of the rate of change of the blowing pressure is proposed. It gives good agreement with experimental data and simulations.

PACS no. 43.25.Ts, 43.75.-z, 43.75.Ef, 43.75.Qr, 43.75.Zz

1. Introduction and problem statement

The phenomenon of register change is well known in recorder-like instruments playing: occuring when the musician blows hard enough in the instrument, it corresponds to a jump between two periodic oscillation regimes synchronised on different resonance modes of the instrument. Thus, a jump from the *first register* to the *second register* (synchronised on the first and the second resonance modes, respectively) is characterised by a frequency leap approximately an octave higher (see for example [1]). Register change is known to be accompanied by hysteresis (see for example [1, 2, 3, 4]): the blowing pressure at which the jump between two registers occurs (the so-called regime change threshold) is higher for rising pressures than for diminishing pressures. As it is related to the selection, through the control of the blowing pressure, of the note played by the instrument, the phenomenon of register change is particularly important for recorder players. A larger hysteresis is moreover related to a greater freedom in terms of musical performance: it allows both to play *forte* on the first register and *piano* on the second register, allowing a wider control in terms of nuance and timbre.

Some studies focused on both the prediction and the experimental detection of regime change thresholds [1, 2, 3]. Other studies focused on the influence of different parameters on regime change thresholds, such as the geometrical dimensions of channel, chamfers and excitation window of recorders or organ flue pipes [5, 6, 7], the importance of nonlinear losses [3], or the convection velocity of perturbations on the jet [3].

Coltman [1, 8] has shown that the study of the linearised model allows to determine the auto-oscillation conditions on the different modes, and thus partially explains the hysteresis phenomenon. A first attempt to explain and predict the register change and hysteresis phenomena through an analysis of the non linearised model for flutes has been proposed by Sawada and Sakaba [2]. However, their results have not been validated through comparison with experimental data. More recent studies have demonstrated that the resolution of the complete non linear model through numerical methods dedicated to computation of periodic solutions allows to explain and

Received 21 March 2014,
accepted 27 August 2014.

* currently at: Gipsa-lab, CNRS, UMR 5216, Grenoble INP, Université Joseph Fourier, Université Stendhal, Grenoble Campus, 11 rue des Mathématiques, BP 46, 38402 Saint Martin d'Héres Cedex, France

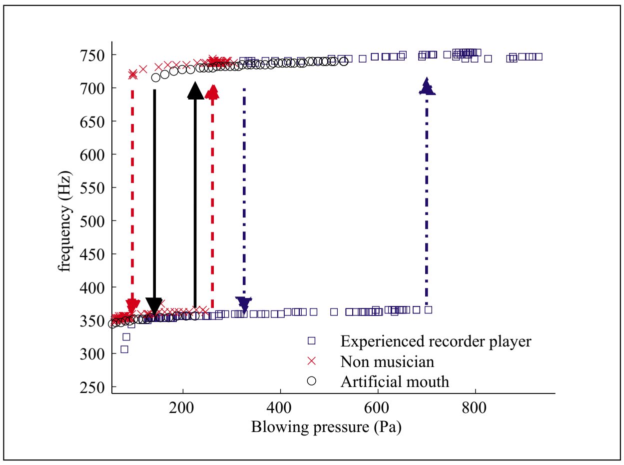

Figure 1. Oscillation frequency with respect to the blowing pressure, for the F_4 fingering of an alto Zen On recorder, played by an experienced recorder player, a non musician and an artificial mouth. Points around 350 Hz and 740 Hz correspond to the first and second register, respectively.

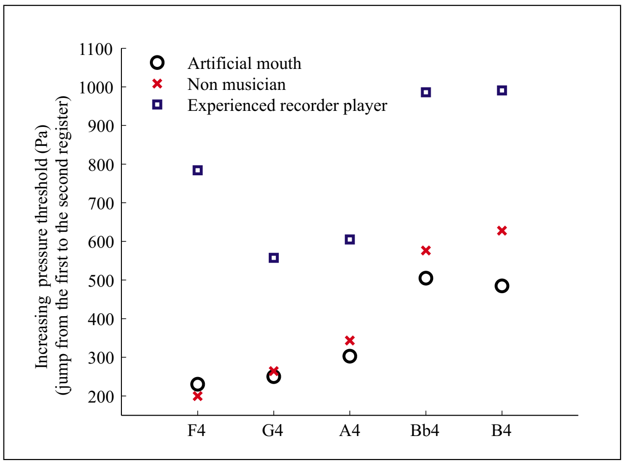

Figure 2. Increasing pressure thresholds corresponding to the jump from the first to the second register of an alto recorder played by an experienced recorder player, a non musician and an artificial mouth, for five fingerings.

predict, under quasi-static hypothesis, the hysteresis associated to register change [9]. Finally, it seems that few studies have focused, in terms of regime change thresholds, on other control parameters (*i.e.* parameters related to the musician) than the slowly varying blowing pressure.

Since it has important musical consequences, one can wonder if recorder players develop strategies to change the values of regime change thresholds and to maximize the hysteresis. To test this hypothesis, increasing and decreasing profiles of blowing pressure (*crescendo* and *decrescendo*) were performed on the same alto recorder and for a given fingering (corresponding to the note F_4), by an experienced recorder player, a non player, and an artificial mouth [10]. Both experienced musician and non musician have been instructed to stay as long as possible on the first register and on the second register for *crescendo* and *decrescendo* respectively. The different experimental setups will be described in Section 2.

The fundamental frequency of the sound is represented with respect to the blowing pressure in Figure 1. The musician is observed to reach increasing and decreasing regime change thresholds respectively 213% higher and 214% higher than the artificial mouth. On the other hand, differences between the non musician and the artificial mouth are of 9% for the increasing threshold and 32% for the decreasing threshold. As highlighted in Figure 2, similar comparisons on other fingerings (G_4, A_4, B_4^b and B_4) show that thresholds reached by the musician are at least 95% higher and up to 240% higher than thresholds observed on the artificial mouth. By contrast, thresholds obtained by the non musician are at most 13.3% lower and 29% higher than thresholds of the artificial mouth. For these increasing thresholds, the values observed on the non musician during the different realisations vary between 6% of the mean values represented in Figure 2 (case of the B_4^b fingering) and 33% of the mean values (case of the F_4 and G_4 fingerings). In the same way, for the experienced recorder player, the

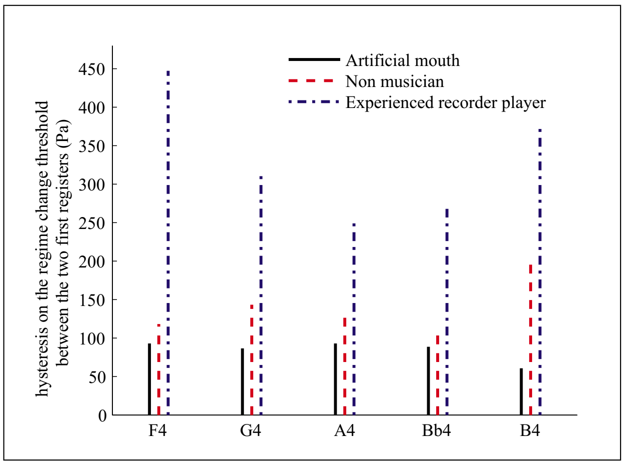

Figure 3. Hysteresis on the jump between the two first registers of an alto recorder played by an experienced recorder player, a non musician and an artificial mouth, for five fingerings.

values observed for the different realisations vary between 5% (F_4 fingering) and 21% (B_4^b fingering) of the mean values.

Figure 3 presents the comparison between the experienced recorder player, the non musician and the artificial mouth in terms of hysteresis. For the three cases, the difference between the thresholds obtained performing increasing and decreasing blowing pressure ramps are represented for the five fingerings studied. The musician is observed to reach hysteresis between 169% and 380% wider than the artificial mouth for the F_4, G_4, A_4 and B_4^b fingerings, and up to 515% wider for the B_4 fingering. The hysteresis observed for the non musician are between 27% and 233% wider than those obtained with the artificial mouth. It is worth noting that the maximum relative difference of 233% is obtained for the B_4 fingering. For all the other fingerings, the relative differences with the artificial mouth remain between 27% and 65%. In all cases, the hysteresis obtained by the experienced recorder player are at least 84% wider than that observed for the non musician.

As a first conclusion, the behaviour of a given instrument played by the artificial mouth and by a non musician can be considered not significantly different in terms of increasing regime change thresholds. In terms of hysteresis, if the results are not significantly different for the F_4, A_4 and B_4^b fingerings, more important differences are observed for both the G_4 and B_4 fingerings. However, the values observed for the experienced recorder player remain significantly higher, both in terms of thresholds and hysteresis, than that obtained for the non player and the artificial mouth. Contrary to the non musician, the experienced recorder player is thus able to significantly and systematically modify these thresholds, and thus to enlarge the hysteresis, which presents an obvious musical interest.

Which parameters does the musician use to control the regime change thresholds?

Even if the influence of the blowing pressure has been widely studied under hypothesis of quasi-static variations [1, 2, 3, 4, 5, 6, 7, 11, 9] (called hereafter *the static case*), and even if studies have focused on the measurement of various control parameters [12, 13, 14], to the authors' knowledge, no study has ever focused on the influence of the blowing pressure *dynamics* (*i.e* the rate of change of the blowing pressure with respect to time) on the behaviour of recorder-like instruments. Recent works have shown the strong influence of this parameter on oscillation thresholds of reed instruments [15, 16], and thus suggest that it could be a control parameter for musicians. Moreover, the comparison between the blowing pressure profiles observed on both the non musician and the experienced recorder player during the *crescendo* (see Figure 4) supports this assumption. Indeed, for the musician, the blowing pressure profiles are smooth and appear to be quite repeatable. The experienced recorder player thus seems to *control* the evolution with time of its blowing pressure. On the other hand, the blowing pressure profiles observed on the non musician seem less repeatable, and exhibit oscillations which appear to be random.

From a more theoretical point of view, as the cause of register change in recorder-like instruments has recently been identified as a bifurcation of the system [4, 9], corresponding to a loss of stability of a periodic solution branch, it suggests to consider the results of dynamic bifurcations theory [17]. This theory takes into account time evolution of the bifurcation parameters.

This paper focuses on the influence of the blowing pressure dynamics on the regime change thresholds between the two first registers of recorder-like instruments, in the case of linearly increasing and decreasing ramps of the blowing pressure. In Section 2, the state-of-the-art physical model for recorder-like instruments is briefly presented, as well as the instrument used for experiments, and the numerical and experimental tools involved in this study. Experimental and numerical results are presented in section 3, highlighting the strong influence of the slope of a linear ramp of the blowing pressure on the thresholds. Finally, a phenomenological modelling of regime change is proposed and validated in Section 4, which allows to predict the values of regime change thresholds and associated hysteresis in the case of a time-varying blowing pressure.

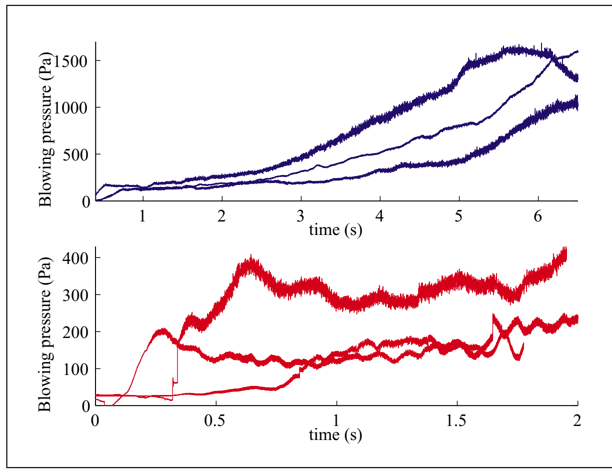

Figure 4. Blowing pressure profiles observed on an experienced recorder player (up) and on a non musician (down), for *crescendo* on different fingerings of an alto recorder. Both the experienced recorder player and the non musician were instructed to stay as long as possible on the first register.

2. Experimental and numerical tools

In this section, experimental and numerical tools used throughout the article are introduced.

2.1. Measurements on musicians

For the present study, an alto *Bressan* Zen-On recorder adapted for different measurements and whose geometry is described in [18] has been played by the professional recorder player Marine Sablonnière. As illustrated in Figure 5, two holes have been drilled to allow a measurement of both the blowing pressure P_m in the musician's mouth, through a capillary tube connected to a pressure sensor Honeywell ASCX01DN, and the acoustic pressure in the resonator (under the labium), through a differential pressure sensor Endevco 8507C-2.

2.2. Pressure controlled artificial mouth

Such experiments with musicians do not allow a systematic and repeatable exploration of the instrument behaviour. To play the instrument without any instrumentalist, a pressure controlled artificial mouth is used [10]. This setup allows to freeze different parameters (such as the configuration of the vocal tract or the distance between the holes and the fingers) which continuously vary when a musician is playing. Compared to other blowing machines used for example in [1, 2, 3], the particularity lies here in the ability to control the blowing pressure in a very precise way. As described in Figure 6, a servo valve connected

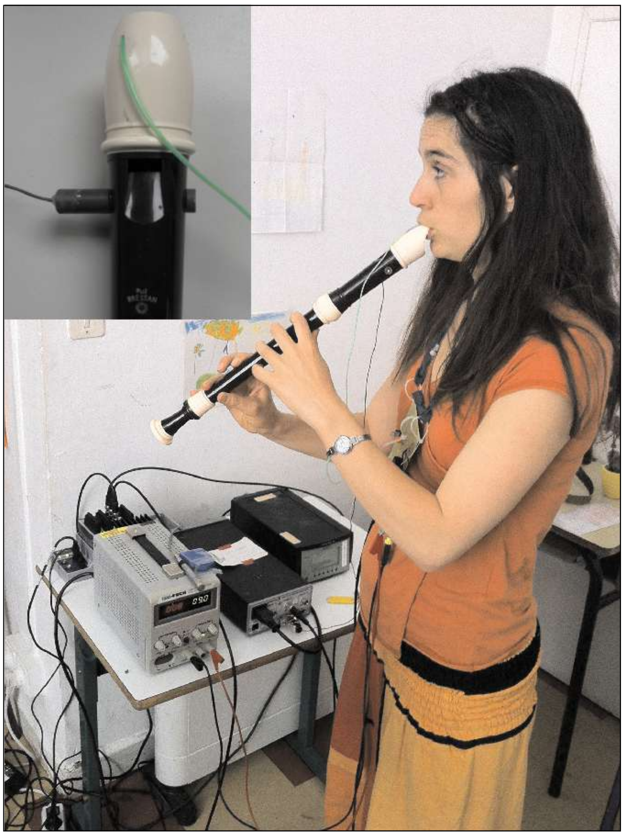

Figure 5. Experimental setup with the adapted alto Zen-On recorder, allowing the measurement of both the pressure in the mouth of the recorder player and the acoustic pressure under the labium.

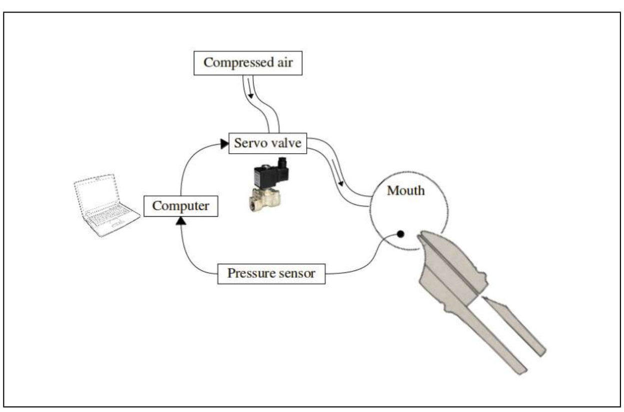

Figure 6. Schematic representation of the principle of the artificial mouth. The opening of the servo valve, controlling the flow injected in the mouth, is adapted every 40 μs in order to minimize the difference between the measured and the desired values of the mouth pressure.

to compressed air controls the flow injected in the instrument through a cavity representing the mouth of the musician, whose volume (about 30 cm^3) corresponds to that of a human vocal tract [10]. Every 40 μs, the desired pressure (the target) is compared to the pressure measured in the mouth through a differential pressure sensor endevco 8507C-1. The electric current sent to the servo valve, directly controlling its opening and thus the flow injected in

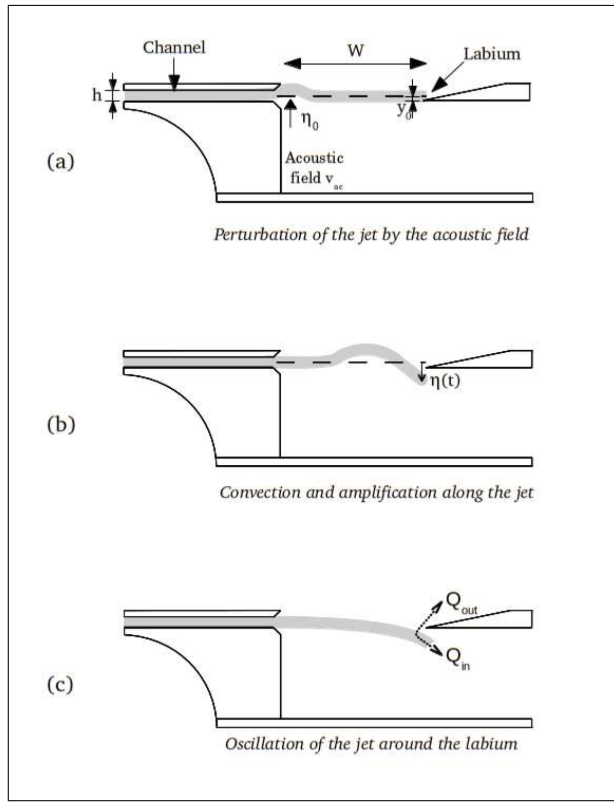

Figure 7. Schematic representation of the jet behaviour, based on Fabre in [21]. (a) Perturbation of the jet at the channel exit by the acoustic field present in the resonator. (b) Convection and amplification of the perturbation, due to the unstable nature of the jet. (c) Jet-labium interaction: oscillation of the jet around the labium, which sustains the acoustic field.

the mouth, is then adjusted using a Proportional Integral Derivative controller scheme. It is implemented on a DSP card dSpace 1006 [10].

2.3. Physical model of the instrument

In parallel with experiments, the behaviour of the state-of-the-art model for recorder-like instruments is studied through time-domain simulations and numerical continuation. The results are qualitatively compared below to experimental data, giving rise to a better understanding of the different phenomena involved.

As for other wind instruments, the mechanism of sound production in recorder-like instruments can be described as a coupling between a nonlinear exciter and a linear, passive resonator, the later being constituted by the air column contained in the pipe [19, 20]. However, they differ from other wind instruments in the nature of their exciter: whereas it involves the vibration of a solid element for reed and brass instruments (a cane reed or the musician's lips), it is constituted here by the nonlinear interaction between an air jet and a sharp edge called *labium* (see for example [21]), as illustrated in Figure 7.

More precisely, the auto-oscillation process is modeled as follows: when the musician blows into the instrument, a jet with velocity U_j and half width b is created at the channel exit. As the jet is naturally unstable, any perturbation is amplified while being convected along the jet, from the channel exit to the labium. The convection velocity c_v of these perturbations on the jet is related to the jet velocity itself through: $c_v \approx 0.4U_j$ [22, 23, 24]. The convection from the channel exit to the labium introduces a delay τ in the system, related both to the distance W between the channel exit and the labium (see Figure 7) and to the convection velocity c_v through: $\tau = W/c_v$. Due to its instability, the jet oscillates around the labium with a deflection amplitude $\eta(t)$, leading to an alternate flow injection inside and outside the instrument. These two flow sources Q_{in} and Q_{out} in phase opposition (separated by a small distance δ_d, whose value is evaluated by Verge in [25]) act as a dipolar pressure source difference $\Delta p_{src}(t)$ on the resonator [1, 25, 26], represented through its admittance $Y(\omega)$.

The acoustic velocity $v_{ac}(t)$ of the waves created in the resonator disrupts back the air jet at the channel exit. As described above, this perturbation is convected and amplified along the jet, toward the labium. The instability is amplified through this feedback loop, leading to self-sustained oscillations. This mechanism of sound production can be represented by a feedback loop system, represented in Figure 8.

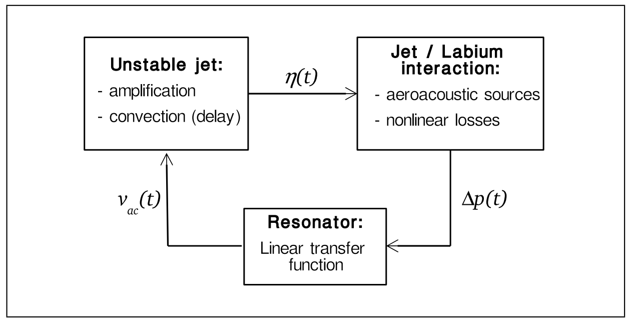

Figure 8. Basic modelling of sound production mechanism in recorder-like instruments, as a system with a feedback loop [28, 21].

According to various studies describing the different physical phenomena involved ([6, 22, 23, 24, 27] for the jet, [1, 25, 26] for the aeroacoustic source), the state-of-the-art model for recorder-like instruments [21] is described through system 1, in which each equation is related to a given element of the feedback loop system of Figure 8,

$$
\begin{aligned}
\eta(t) &= \frac{h}{U_j} \mathrm{e}^{\alpha_i W} v_{ac}(t-\tau), &(1)\\
\Delta p(t) &= \Delta p_{src}(t) + \Delta p_{los}(t) \\
&= \frac{\rho \delta_d b U_j}{W} \frac{d}{dt} \left[\tanh\left(\frac{\eta(t) - y_0}{b} \right) \right] &(2)\\
&\quad - \frac{\rho}{2} \left(\frac{v_{ac}(t)}{\alpha_{vc}} \right)^2 \operatorname{sgn}\left(v_{ac}(t)\right), \\
V_{ac}(\omega) &= Y(\omega) \cdot P(\omega) \\
&= \left[\frac{a_0}{b_0 j\omega + c_0} \right. &(3)\\
&\quad \left. + \sum_{k=1}^{p-1} \frac{a_k \mathrm{j}\omega}{\omega_k^2 - \omega^2 + \mathrm{j}\omega \frac{\omega_k}{Q_k}} \right] P(\omega).
\end{aligned}
$$

In these equations, α_i is an empirical coefficient characterizing the amplification of the jet perturbations [22, 27], ρ is the air density, and y_0 the offset between the labium position and the jet centerline (see Figure 7). V_{ac} and P are respectively the frequency-domain expressions of the acoustic velocity at the pipe inlet $v_{ac}(t)$ and the pressure source $\Delta p(t)$.

In the second equation, the additional term $\Delta p_{los} = -(\rho/2)(v_{ac}(t)/\alpha_{vc})^2 \operatorname{sgn}(v_{ac}(t))$ models nonlinear losses due to vortex shedding at the labium [29]. α_{vc} is a *vena contracta* factor (estimated at 0.6 in the case of a sharp edge), and sgn represents the sign function.

The admittance $Y(\omega)$ is represented in the frequency-domain as a sum of resonance modes, including a mode at zero frequency (the so-called uniform mode [28]). The coefficients a_k, ω_k and Q_k are respectively the modal amplitude, the resonance pulsation and the quality factor of the k^{th} resonance mode, ω is the pulsation, and a_0, b_0 and c_0 are the coefficients of the uniform mode. For the different fingerings of the recorder used for experiments, these coefficients are estimated through a fit of the admittance. These admittances are estimated through the measurement of the geometrical dimensions of the bore of the recorder and the use of the software WIAT [30]. The length corrections related to the excitation window of the recorder (see Figure 7) are subsequently taken into account using the analytical formulas detailed in chapter 7 of [28].

2.3.1. Numerical resolution methods

Time-domain simulations of this model are carried out through a classical Runge-Kutta method of order 3, implemented in Simulink [31]. A high sampling frequency $f_s = 23 \times 44100$ Hz is used. This value is chosen both because the solution is not significantly different for higher sampling frequencies, and because it allows an easy re-sampling at a frequency suitable for audio production systems.

In parallel, equilibrium and periodic steady-state solutions of the model are computed using orthogonal collocation (see for example [32]) and numerical continuation [33]. Starting from a given equilibrium or periodic solution, continuation methods, which rely on the implicit function theorem [34], compute the neighbouring solution, *i.e* the solution for a slightly different value of the parameter of interest (the so-called continuation parameter), using a prediction-correction method. This iterative process is schematically represented in Figure 9. It thus aims at following the corresponding branch (that is to say "family") of solutions when the continuation parameter varies. For more details on these methods and their adaptation to the state-of-the-art recorder model, the reader is referred to [35, 36] and [9]. The stability properties of the different parts of the branches are subsequently determined using the Floquet theory (see for example [37]).

For a given dynamical system, the computation of both the different branches of equilibrium and periodic solutions and their stability, here achieved with the software DDE-Biftool [38, 39, 36], leads to bifurcation diagrams. Such diagrams ideally represent all the branches of equilibrium and periodic solutions as a function of the continuation parameter. Moreover, they provide specific information on unstable parts of the branches, coexistence of different solutions, and bifurcations arising along the different branches. It is not possible to access this information experimentally or through time integration methods.

Thereby, a bifurcation diagram provides a more global knowledge on the different possible solutions of the system, and an easier interpretation of different phenomena observed experimentally or in time-domain simulations, as illustrated for example in [40, 41, 9]. This will be illustrated by Figure 12 provided in section 3, which represents such a diagram of the state-of-the-art model of flute-like instruments, in terms of oscillation frequency of the periodic solutions with respect to the blowing pressure.

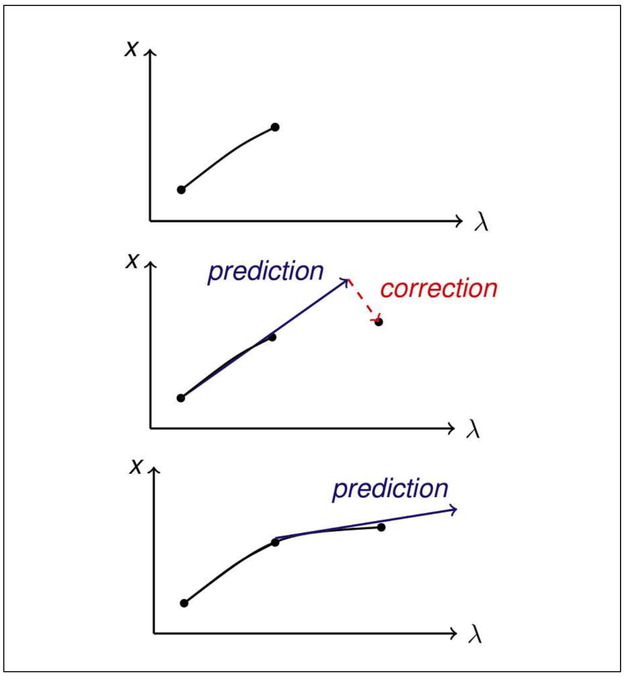

Figure 9. Schematic representation of the principle of numerical continuation through a prediction-correction algorithm [33, 38]. Starting from a known part of the branch, the neighbouring solution (for a slightly different value of the continuation parameter λ) is predicted and corrected. By succesive iterations, it leads to the computation of the complete solution branch of equilibrium or periodic solutions. x represents a characteristic of the solution, such as its frequency or its amplitude.

3. Linear ramps of the blowing pressure: experimental and numerical results

3.1. Influence of the slope of blowing pressure ramps on thresholds

As highlighted in Section 1, important differences arise, in terms of regime change thresholds and hysteresis, between experienced recorder player and artificial mouth or non musician, which remain unexplained. Recent works [15, 16] have demonstrated the strong influence of the dynamics of control parameters on the oscillation threshold of reed instruments. Particularly, it has highlighted, in such instruments, the phenomenon of *bifurcation delay*, corresponding to a shift of the oscillation threshold caused by the dynamics of the control parameter [17]. Although we focus here on transitions between the two first registers (i.e. between two different oscillation regimes), and although recorder-like instruments are mathematically quite different dynamical systems from reed instruments, these former studies suggest that the temporal profile $P_m(t)$ of the pressure dynamics could influence the regime change thresholds. We focus in this Section on the comparison of regime change thresholds between the *static case* and the *dynamic case*, the latter corresponding to a time varying blowing pressure.

To test this hypothesis, linearly increasing and decreasing blowing pressure ramps $P_m(t) = P_{ini} + a \cdot t$, with different slopes a, have been run both through time-domain simulations and experiments with the artificial mouth. Figure 10 represents, for the F_4 fingering, the *dynamic* pressure thresholds P_{dyn} corresponding to the jump between the two first registers, with respect to the slope a. The positive and negative values of a correspond to increasing and decreasing ramps of $P_m(t)$, respectively. For each value of a, the experimental threshold is a mean value calculated for three realisations of the considered ramps. In this paper, the value of P_{dyn} is determined through a fundamental frequency detection using the software Yin [42]: P_{dyn} is defined as the value of P_m at which a jump of the fundamental frequency is observed. The temporal resolution of the detection is $0.0016\ s$ for experimental signals and $0.0007\ s$ for simulation signals, which corresponds to a resolution of 0.8 and 0.36 Pa (respectively), in the case of a slope $a = 500\ Pa/s$ of the blowing pressure. Moreover, for a given value of a and a given fingering, the thresholds measured for the different realisations differ typically no more than 5% from their mean value.

Despite the dramatic simplifications of the model, these first results presented in Figure 10 higlight that the real instrument and the model present similar qualitative behaviours. Surprisingly enough, the behaviours observed numerically in time-domain simulation and experimentally with the artificial mouth are also quantitatively similar, with typical relative differences between 3% and 28% on the thresholds observed for rising pressure (called *increasing pressure threshold* $P_{dyn\ 1\to2}$). For the *decreasing pressure threshold* $P_{dyn\ 2\to1}$, observed for diminishing pressure, the difference is more important, with a typical relative deviation of about 50%.

Furthermore, the strong influence of a on both $P_{dyn\ 1\to2}$ and $P_{dyn\ 2\to1}$ is clearly pointed out: with the artificial mouth, $|a| = 400$ Pa/s leads to a value of $P_{dyn\ 1\to2}$ 45% higher than $|a| = 10$ Pa/s, and to a value of $P_{dyn\ 2\to1}$ 16% lower. Similarly, for time-domain simulations, $|a| = 400$ Pa/s leads to a value of $P_{dyn\ 1\to2}$ 15.5% higher and

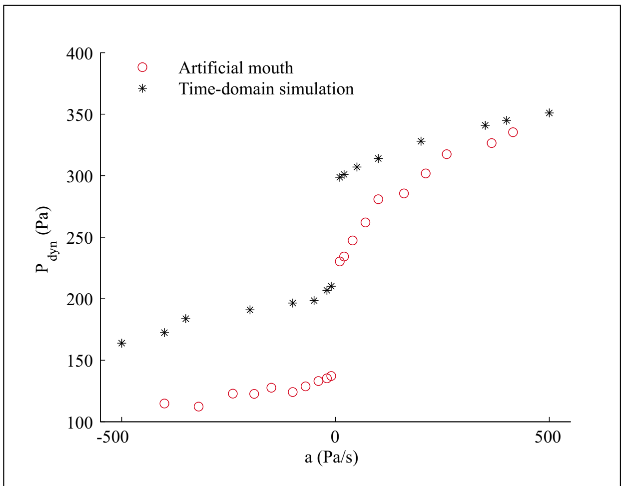

Figure 10. Dynamic regime change threshold between the two first registers of the F_4 fingering, with respect to the slope a of linear ramps: artificial mouth and time-domain simulation.

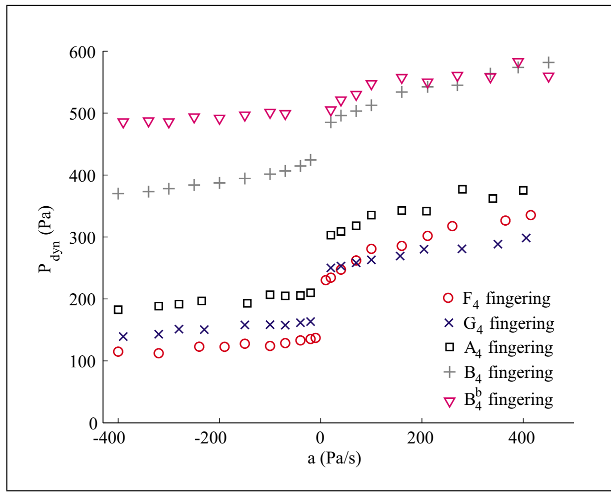

Figure 11. Transition between the two first registers of an alto recorder played by an artificial mouth, for five different fingerings: representation of the dynamic regime change thresholds with respect to the slope a of linear ramps of the blowing pressure.

to a value of $P_{dyn\ 2\to 1}$ 18% lower than $|a| = 10$ Pa/s. As $P_{dyn\ 1\to 2}$ and $P_{dyn\ 2\to 1}$ are respectively increased and decreased, increasing a thus enlarges the hysteresis. This can be compared (at least qualitatively) with phenomena observed on an experienced recorder player, presented in Section 1.

Figure 11 represents, as previously, the mean value of the regime change thresholds $P_{dyn\ 1\to 2}$ and $P_{dyn\ 2\to 1}$ obtained for three experiments, with respect to the slope a, for the other fingerings already studied in Section 1. It higlights that the behaviour observed in Figure 10 for the F_4 fingering looks similar for other fingerings of the recorder. Indeed, depending on the fingering, the increase of $|a|$ from 20 Pa/s to 400 Pa/s leads to an increase of $P_{dyn\ 1\to 2}$ between 13% and 43% and to a decrease of $P_{dyn\ 2\to 1}$ from 3% to 15%. Again, these results can be qualitatively compared with the results presented in Section 1 for an experienced recorder player.

3.2. Influence of the slope of blowing pressure ramps on oscillation frequency and amplitude

As observed for the oscillation threshold in clarinet-like instruments [15], we show in this section that a modification of the regime change threshold does not imply a strong modification of the characteristic curves, observed in the *static case*, linking the oscillation amplitude and the oscillation frequency to the blowing pressure. For numerical results, this feature can be easily illustrated through a comparison between the results of time-domain simulations and the bifurcation diagrams obtained through numerical continuation. This is done in Figure 12, in terms of fundamental frequency with respect to the blowing pressure P_m, for modal coefficients corresponding to the G_4 fingering. In this figure, the two periodic solution branches correspond to the first and the second registers, and solid lines with crosses and dashed lines represent stable and unstable parts of the branches, respectively. As the computation of such a bifurcation diagram relies on the static bi-

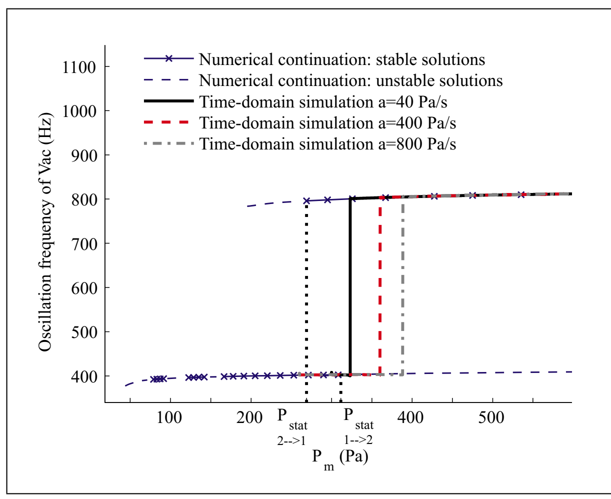

Figure 12. Bifurcation diagram of the G_4 fingering, superimposed with time-domain simulations of increasing linear ramps of the blowing pressure, for different values of the slope a: representation of the oscillation frequency with respect to the blowing pressure P_m. For the bifurcation diagram, the two branches correspond to the first and the second register, solid lines with crosses and dashed lines represent stable and unstable parts of the branches, respectively. The vertical dotted lines highlight the static regime change thresholds $P_{stat\ 1\to 2}$ and $P_{stat\ 2\to 1}$.

furcation theory, the point where the first register becomes unstable, at $P_m = 311.5$ Pa, corresponds to the *static threshold* $P_{stat\ 1\to 2}$ from first to second register. It thus corresponds to the threshold that would be observed, in time-domain simulation, by choosing successive constant values of the blowing pressure, and letting the system reach a steady-state solution (here, the first or the second register). Similarly, the point at which the change of stability of the second register is observed corresponds to the static threshold from second to first register $P_{stat\ 2\to 1} = 259$ Pa.

Figure 12 shows that for high values of a, the system follows the unstable part of the branch corresponding to the first register: the maximum relative difference between the frequency predicted by the bifurcation diagram and the results of time-domain simulations is 9 cents. In the *dynamic case*, the system thus remains, at least for a while, on the periodic solution branch corresponding to the "starting" regime (the first register in Figure 12), after it became unstable.

Providing, for the A fingering, the oscillation amplitude as a function of P_m for different values of a, Figure 13 highlights that the same property is observed experimentally. In both cases, the value of a considerably alters the register change thresholds. However, far enough from the jump between the two registers, the oscillation amplitude only depends on the value of P_m, and does not appear significantly affected by the value of a.

In Figure 13, the comparison between the two slowest ramps (20 Pa/s and 100 Pa/s) and the two others (280 Pa/s and 340 Pa/s) is particularly interesting. Indeed, for the two slowest ramps, an additional oscillation regime, corresponding to a quasiperiodic sound (called *multiphonic sound* in a musical context) [7, 8, 43, 4, 44], is observed for blowing pressure between 300 Pa and 400 Pa for a = 20 Pa/s, and between 340 and 400 Pa for a = 100 Pa/s. As this regime does not appear for higher slopes, it highlights that a modification of the blowing pressure dynamics can allow the musician to avoid (or conversely to favor) a given oscillation regime.

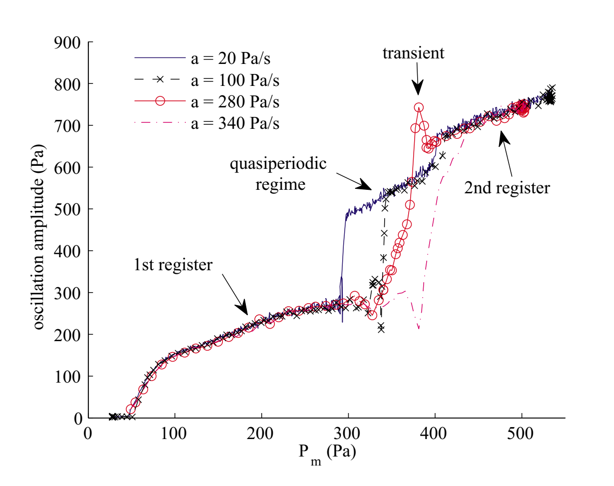

Figure 13. Increasing linear ramps of the blowing pressure, with different slopes a, achieved with an artificial mouth: oscillation amplitude observed for the A_4 fingering of an alto recorder, with respect to the blowing pressure.

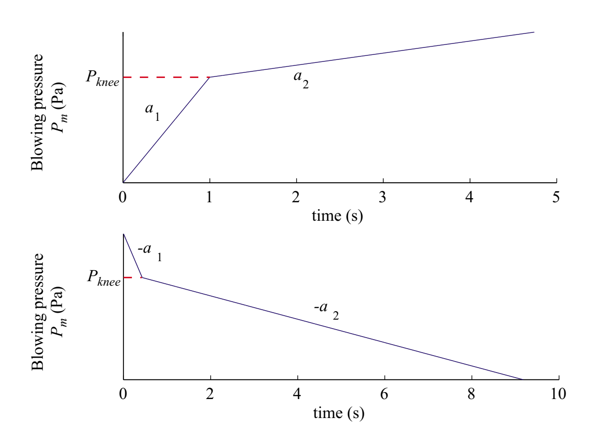

Figure 14. Schematic representation of the piecewise linear ramps of the blowing pressure, achieved in time-domain simulation and experimentally with the artificial mouth. For both increasing ramps (up) and decreasing ramps (down), the slope of the blowing pressure ramp is a_1 before the value P_{knee} has been reached, and a_2 after P_{knee} has been reached.

3.3. Influence of the pressure dynamics before the static threshold

To better understand the mechanisms involved in the case of a *dynamic* bifurcation between two registers, this section focuses on the influence, on the regime change thresholds, of the evolution of $P_m(t)$ before the *static* threshold P_{stat} has been reached. In other words, the aim is to determine whether the way $P_m(t)$ evolves before the static threshold is reached impacts the *dynamic* regime change threshold.

To investigate this issue, different piecewise linear ramps have been achieved both with the artificial mouth and in time-domain simulation. As illustrated in Figure 14, these profiles are defined for rising pressures such as $\mathrm{d}P_m/\mathrm{d}t = a_1$ for $P_m < P_{knee}$ and $\mathrm{d}P_m/\mathrm{d}t = a_2$ for $P_m > P_{knee}$ (where a_1 and a_2 are constants) and P_{knee} is a constant that may be adjusted. For diminishing pressures, they are such as $\mathrm{d}P_m/\mathrm{d}t = -a_1$ for $P_m > P_{knee}$ and $\mathrm{d}P_m/\mathrm{d}t = -a_2$ for $P_m < P_{knee}$.

3.3.1. Experimental results

Experimentally, blowing pressure profiles constituted by two linear ramps with different slopes ($|a_1| = 350$ Pa/s, $|a_2| = 40$ Pa/s) have been achieved for the G_4 fingering. The pressure P_{knee} at which the knee break occurs varies between the different realisations.

Figure 15 presents these experimental results in terms of $P_{dyn\ 1\to2}$ and $P_{dyn\ 2\to1}$, with respect to $P_{knee} - P_{stat}$. Thereby, a zero abscissa corresponds to a change of slope from a_1 to a_2 at a pressure equal to $P_{stat\ 1\to2}$ for rising pressure, and equal to $P_{stat\ 2\to1}$ for diminishing pressure. It highlights that for rising pressure, $P_{dyn\ 1\to2}$ remains constant as long as $P_{knee} < P_{stat\ 1\to2}$ (i.e. for negative values of the abscissa), and that this constant value (about 258 Pa) corresponds to the value of $P_{dyn\ 1\to2}$ previously observed for a linear ramp with constant slope $a_2 = 40$ Pa/s (see Figure 11). Conversely, once $P_{knee} > P_{stat\ 1\to2}$, the value of $P_{dyn\ 1\to2}$ gradually increases to reach 295 Pa, which corresponds to the value observed for a linear ramp with a contant slope $a_1 = 350$ Pa/s.

The same behaviour is observed for the *decreasing* threshold: as long as $P_{knee} > P_{stat\ 2\to1}$, the value of $P_{dyn\ 2\to1}$ is almost contant and close to that observed previously for a linear ramp of constant slope $a_2 = -40$ Pa/s (see Figure 11). However, for $P_{knee} < P_{stat\ 2\to1}$, the value of $P_{dyn\ 2\to1}$ progressively decreases to about 142 Pa, which

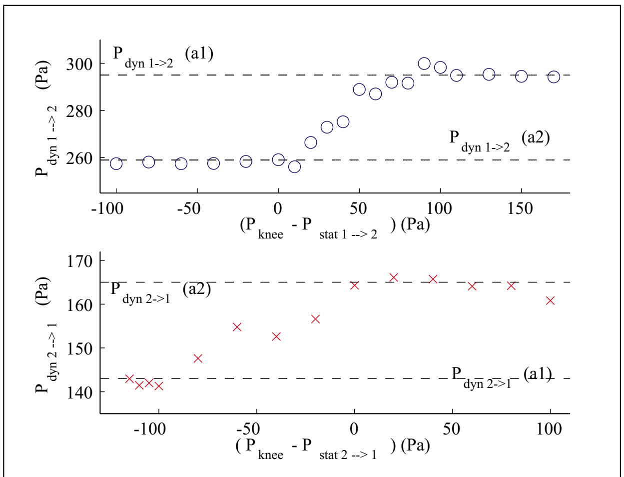

Figure 15. Piecewise linear ramps of the blowing pressure ($a_1 = 350$ Pa/s and $a_2 = 40$ Pa/s), achieved on the G_4 fingering of an alto recorder played by an artificial mouth. Ordinate: dynamic threshold $P_{dyn\ 1\to 2}$ (up) and $P_{dyn\ 2\to 1}$ (down). Abscissa: difference between the pressure P_{knee} at which the knee occurs and the static regime change threshold P_{stat}. Dashed lines represent the dynamic regime change thresholds observed previously for linear ramps of constant slope a_1 and a_2 respectively.

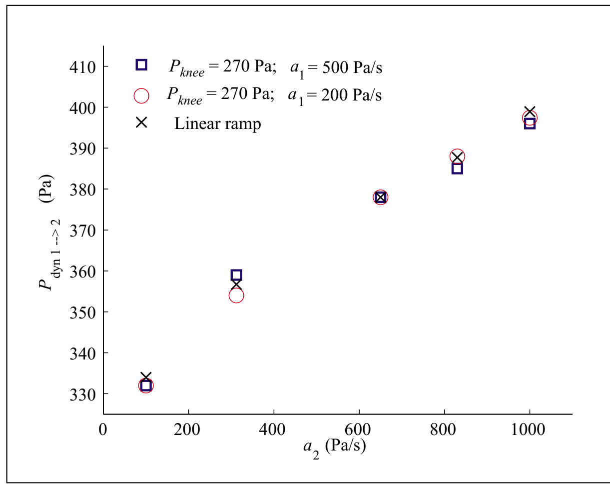

Figure 16. Time-domain simulations of piecewise linear ramps of the blowing pressure with $P_{knee} = 270$ Pa ($a_1 = 500$ Pa/s for squares and $a_1 = 200$ Pa/s for circles) and of linear ramps of the blowing pressure (crosses). Representation of the increasing dynamic regime change threshold $P_{dyn\ 1\to 2}$ for the G_4 fingering, as a function of a_2 (slope of the second part of the blowing pressure profile for piecewise linear ramps, and slope of the linear ramps).

corresponds to that observed for a linear ramp of constant slope $a_1 = -350$ Pa/s (see Figure 11).

As a conclusion, as long as the slope break occurs before the static threshold has been reached, the dynamic threshold is driven by the slope of the second part of the blowing pressure profile. If it occurs just after the static threshold has been reached, the dynamic threshold lies between the dynamic thresholds corresponding to the two slopes of the blowing pressure profile. Finally, if the slope break occurs, for rising pressure, at a presure sufficiently higher (respectively lower for diminishing pressure) than the static threshold, the dynamic threshold is driven, as expected, by the slope of the first part of the blowing pressure profile.

3.3.2. Results of time-domain simulations

These experimentally observed behaviours are also observed on numerical simulations of the model. For modal coefficients corresponding to the G_4 fingering, the comparison has been made between the dynamic thresholds obtained for three different cases:

- linear increasing ramps of $P_m(t)$, with slope a_2.
- a first piecewise linear increasing ramp, with a slope change at $P_{knee} = 270$ Pa, and a fixed value of $a_1 = 500$ Pa/s.
- a second piecewise linear increasing ramp, with a slope change at $P_{knee} = 270$ Pa, and a fixed value of $a_1 = 200$ Pa/s.

It is worth noting that for the two kinds of piecewise linear ramps, P_{knee} is lower than $P_{stat\ 1\to 2}$, predicted by a bifurcation diagram at 311.5 Pa (see Figure 12). For each case, various simulations were achieved, for different values of a_2.

Figure 16 provides the comparison of value of $P_{dyn\ 1\to 2}$ obtained for these three kinds of blowing pressure profiles, as a function of a_2. With a maximum relative difference of 0.8%, the thresholds obtained for the piecewise linear profiles are strongly similar to those obtained with linear ramps. As for the experimental results, if $P_{knee} < P_{stat\ 1\to 2}$, the dynamic threshold $P_{dyn\ 1\to 2}$ is thus driven by the second slope a_2 of the profile.

For the particular profile in which $a_1 = 500$ Pa/s and $a_2 = 830$ Pa/s, the influence of the value of P_{knee} on $P_{dyn\ 1\to 2}$ has been studied. The results are represented in Figure 17 in the same way as the experimental results in Figure 15. As experimentally, if $P_{knee} < P_{stat\ 1\to 2}$, the value of $P_{dyn\ 1\to 2}$ is driven by a_2, and a constant threshold of about 388 Pa is observed, corresponding to the value obtained for a linear ramp with a slope equal to $a_2 = 830$ Pa (see figure 16). Conversely, when $P_{knee} > P_{stat 1\to 2}$, $P_{dyn 1\to 2}$ gradually shifts to finally achieve the value of 369 Pa, equal to that oberved for a linear ramp with a slope equal to $a_1 = 500$ Pa/s. The dynamic threshold is then driven by a_1.

3.4. Comparison with the results of an experienced musician

The strong influence of the dynamics of $P_m(t)$ on thresholds and hysteresis suggests, by comparison with results presented in section 1, that musicians could use this property to access to a wider control in terms of nuances and timbre. However, the comparison between the musician and the artificial mouth (see Figures 2, 3 and 11) shows that the values of $P_{dyn\ 1\to 2}$ obtained by the musician remains, for the different fingerings studied, between 61% and 134% higher than the maximal thresholds obtained with the artificial mouth for high values of the slope a.

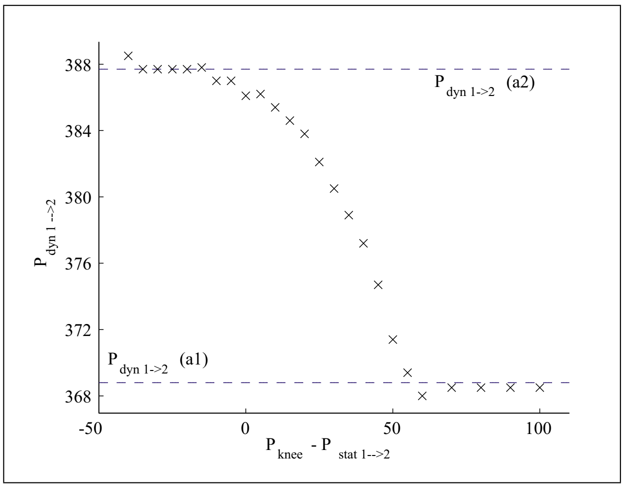

Figure 17. Time-domain simulations of piecewise linear ramps of the blowing pressure (a_1 = 500 Pa/s and a_2 = 830 Pa/s), for the G_4 fingering. Ordinate: dynamic threshold $P_{dyn\ 1\rightarrow 2}$. Abscissa: difference between the pressure P_{knee} at which the knee occurs and the static regime change threshold $P_{stat\ 1\rightarrow 2}$. Dashed lines represent the values of $P_{dyn\ 1\rightarrow 2}$ previously observed for linear ramps of slope a_1 and a_2.

In the same way, the hysteresis obtained by the musician remains between 26% and 102% wider than the maximal hysteresis observed with the artificial mouth for the F_4, G_4, A_4 and B_4^b fingerings, and up to 404% wid er for the B_4 fingering.

3.5. Discussion

These results bring out the strong influence of the dynamics of the blowing pressure on the oscillation regime thresholds in recorder-like instruments. Comparisons between experimental and numerical results show that the substantial simplifications involved in the state-of-the-art physical model of the instrument do not prevent it to faithfully reproduce the phenomena observed experimentally. Suprisingly enough, different numerical results show good agreement not only qualitatively but also quantitatively with the results obtained with the artificial mouth.

Moreover, both the experimental and numerical results show that the *dynamic* threshold does not depend on the dynamics of the blowing pressure before the static threshold has been reached.

Although the system studied here is mathematically very different from one that models reed instruments (see for example [3, 45, 9]), and although focus is set here on bifurcations of periodic solutions, results can be compared with some phenomena highlighted by Bergeot *et al.* on the dynamic oscillation threshold of reed instruments [16, 15]. As in the work of Bergeot, phenomena highlihted are not predicted by the *static* bifurcation theory, often involved in the study of musical instruments.

However, as underlined in Section 3.4, consideration of the blowing pressure dynamics alone is not sufficient to reach the thresholds and hysteresis obtained by an experienced recorder player. Moreover, the thresholds shift observed both in time-domain simulation and on the artificial mouth are temporary, in the sense that the regime change is *delayed* but can not be *avoided* once the static threshold has been exceeded. In the case of the experienced recorder player, it cannot be ruled out that the musician might be able to maintain the oscillation on the desired regime as long as he desires, which would correspond to a *permanent* character of the threshold shift. Both because musicians adapt permanently all the parameters available, and because the measured blowing pressure profiles are much more complex than those studied with the artificial mouth, it is not possible to provide a precise answer to this issue.

The comparison between the results obtained with the artificial mouth and with an experienced recorder player thus suggests that experienced recorder players develop strategies to combine the effects of the dynamics of the blowing pressure with those of other control parameters (such as for example the vocal tract, whose influence on regime change thresholds has been recently studied [46]) in order to enlarge the hysteresis associated to regime change. Moreover, the study presented here focuses on linear profiles of the mouth pressure. As such a temporal evolution does not seem realistic in a musical context (see Section 1 and for example [47, 13]), it would be interesting to consider the effect of more complex temporal evolutions of the blowing pressure.

These different points are thus arguments in favor of consideration of the influence of other control parameters on regime change thresholds and hysteresis. Among others, different works on flute-like instruments [48, 46], together with different studies on other wind instruments [49, 50, 51, 52] suggests that the vocal tract can also influence the regime change thresholds.

4. Toward a phenomenological model of register change

The different properties of the register change phenomenon, observed both experimentally and in simulations in the previous part, allow to propose a preliminary phenomenological modelling of this phenomenon. The aim is not here to propose a method to analyse the physical model of flute-like instruments, which allows to explain and predict the regime change, as Coltman [1, 8], Sawada and Sakaba [2], Auvray *et al.* [3] and Terrien *et al.* [9]. Conversely, a phenomenological modelling of the influence of the blowing pressure *dynamics* on the regime change threshold is proposed.

4.1. Proposed model

Starting from the results presented in figures 15, 16, and 17, which lead to the conclusion that P_{dyn} only depends on the dynamics of the blowing pressure *after* the static threshold has been reached, this modelling is based on the following hypothesis:

- The *regime change* starts when $P_m(t) = P_{stat}$.
- The regime change is not instantaneous, and has a duration t_{dyn} during which the blowing pressure evolves from P_{stat} to P_{dyn}.

We thus write P_{dyn} as the sum of the static threshold P_{stat} and a correction term P_{corr} related to the dynamics of the blowing pressure,

$$P_{dyn} = P_{stat} + P_{corr}. \tag{4}$$

Based on the two hypothesis cited above, a new dimensionless quantity is introduced: the *fraction of regime change* $\zeta(t)$. By definition, $\zeta = 0$ when the regime change has not started (*i.e.* when $P_m(t) < P_{stat}$ for rising pressure and when $P_m(t) > P_{stat}$ for diminishing pressure), and $\zeta = 1$ when the regime change is completed (*i.e.* when $P_m(t) = P_{dyn}$, which corresponds to the change of fundamental frequency, as defined in the previous section). ζ is consequently defined as

$$\zeta(t) = \int_{t_{stat}}^{t} \frac{\partial \zeta}{\partial t}\, \mathrm{d}t, \tag{5}$$

where t_{stat} is the instant at which $P_m(t) = P_{stat}$. Defining the origin of time at t_{stat} leads to $\hat{t} = t - t_{stat}$, and thus gives

$$\zeta(\hat{t}) = \int_{0}^{\hat{t}} \frac{\partial \zeta}{\partial \hat{t}}\, \mathrm{d}\hat{t}. \tag{6}$$

As a simplifying assumption, it is assumed in a first stage that the rate of change $\partial\zeta/\partial\hat{t}$ of the variable $\zeta(\hat{t})$ only depends on the gap $\Delta P(\hat{t}) = P_m(\hat{t}) - P_{stat}$ between the mouth pressure $P_m(\hat{t})$ and the static regime change threshold,

$$\frac{\partial \zeta}{\partial \hat{t}} = f(\Delta P), \tag{7}$$

where f is an unknown monotonous and continuous function.

According to the latest hypothesis, function f can be estimated at different points through the realisation of "steps" profiles of $P_m(t)$, from a value lower than $P_{stat\ 1\to 2}$, to a value larger than $P_{stat\ 1\to 2}$ (see Figure 18). Indeed, in such a case, for a step occuring at $\hat{t} = 0$, $\Delta P(\hat{t})$ corresponds to the difference between the pressure at the top of the step and $P_{stat\ 1\to 2}$, and is thus constant for $\hat{t} > 0$. Consequently, $f(\Delta P)$ is constant with respect to time. From Equations (6) and (7), one thus obtains for blowing pressure steps:

$$\begin{aligned} \zeta(\hat{t}) &= \int_0^{\hat{t}} f(\Delta P)\, \mathrm{d}\hat{t} \\ &= f(\Delta P) \int_0^{\hat{t}} \mathrm{d}\hat{t} \\ &= f(\Delta P) \cdot \hat{t}. \end{aligned} \tag{8}$$

Recalling that $\hat{t}_{dyn}$ is the instant at which $P_m(\hat{t}) = P_{dyn}$, we have by definition $\zeta(\hat{t}_{dyn}) = 1$, and finally obtain for blowing pressure steps

$$f(\Delta P) = \frac{1}{\hat{t}_{dyn}}. \tag{9}$$

For each value of the step amplitude, a different value of $\hat{t}_{dyn}$ is obviously measured through a frequency detection:

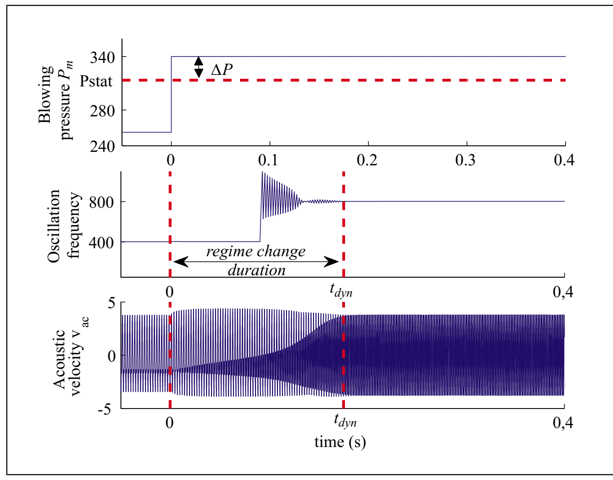

Figure 18. Illustration of the step profiles of the blowing pressure (up) achieved in time-domain simulations, of the detection of the transient duration $\hat{t}_{dyn}$ (middle) and of the corresponding acoustic velocity signal (down).

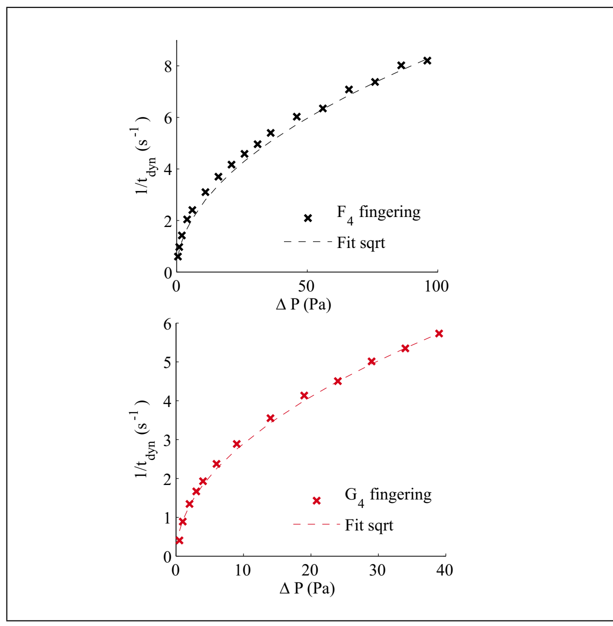

Figure 19. Estimation of the function $f(\Delta P)$: representation of the inverse of the transient duration for step profiles of the blowing pressure, for both the F_4 and G_4 fingerings (left and right respectively), with respect to the difference ΔP between the target pressure of the steps and the static threshold $P_{stat\ 1\to 2}$. Dashed lines represent fit of the data with square root functions.

$\hat{t}_{dyn}$ is defined as the time after which the oscillation frequency varies no more than two times the frequency resolution. Therefore, successive time-domain simulations of P_m steps (see Figure 18) with different amplitudes are carried out, to determine the function $f(\Delta P)$ through Equation (9). Such simulations have been achieved for the two fingerings F_4 and G_4, in both cases for transitions from the first to the second register. The results are represented in Figure 19 with respect to ΔP.

In the two cases, it seems that the results follow a square root function: the linear correlation coefficients between

ΔP and $(1/t_{dyn})^2$ are of 0.96 for the F_4 fingering and 0.97 for the G_4 fingering. Such results thus suggest to approximate the function f through

$$f(\Delta P) = \alpha\sqrt{(\Delta P)}, \tag{10}$$

where the coefficient α depends on the considered fingering.

4.2. Assessment of the model

To check the validity of this modelling, the case of the linear pressure ramps studied in the previous section is now examined. In such a case, the difference between the blowing pressure and the static threshold is defined through $\Delta P(\hat{t}) = a \cdot \hat{t}$, where a is the slope of the ramp in Pa/s. Recalling that $\zeta(\hat{t}_{dyn}) = 1$ and injecting Equations (7) and (10) in Equation (6) leads to

$$\begin{aligned}
&\int_0^{\hat{t}_{dyn}} f(\Delta P(\hat{t}))\,\mathrm{d}\hat{t} = 1,\\
&\int_0^{\hat{t}_{dyn}} \alpha\sqrt{\Delta P(\hat{t})}\,\mathrm{d}\hat{t} = 1,\\
&\int_0^{\hat{t}_{dyn}} \alpha\sqrt{a\hat{t}}\cdot\,\mathrm{d}\hat{t} = 1,\\
&\int_0^{\hat{t}_{dyn}} \sqrt{\hat{t}}\,\mathrm{d}\hat{t} = \frac{1}{\alpha\sqrt{a}},\\
&\hat{t}_{dyn} = \left(\frac{3}{2\alpha\sqrt{a}}\right)^{2/3}.
\end{aligned} \tag{11}$$

Moreover, due to the expression of $\Delta P(\hat{t})$ in the case of linear ramps, one can write from Equations (4) and (11)

$$\begin{aligned}
P_{corr} &= P_{dyn} - P_{stat} = \Delta P(\hat{t}_{dyn})\\
&= a\cdot\hat{t}_{dyn} = \left(\frac{3}{2\alpha}a\right)^{2/3}.
\end{aligned} \tag{12}$$

According to this modelling, the value of P_{corr} obtained with linear ramps should be proportional to the slope a to the power 2/3. Time-domain simulations for linear ramps of $P_m(t)$ with slope a are performed for two fingerings (F_4 and G_4). Figure 20 represents the threshold P_{dyn} corresponding to the end of the transition from the first to the second register with respect to the slope a power 2/3. The results are correctly fitted by straight lines, with correlation coefficients higher than 0.99. This good agreement with the model prediction (Equation 12) thus allows to validate the proposed modelling of the phenomenon of regime change. Moreover, on such a representation, the intercept of the fit with the y-axis provides a prediction of the static regime change threshold, which can not be exactly determined, strictly speaking, with linear ramps of the blowing pressure. The static thresholds thereby obtained are 294 Pa and 314 Pa for the F_4 and G_4 fingering respectively. These values present relative differences of 0.1% and 0.8% with the thresholds of 294.3 Pa and 311.5 Pa predicted by the bifurcation diagrams computed

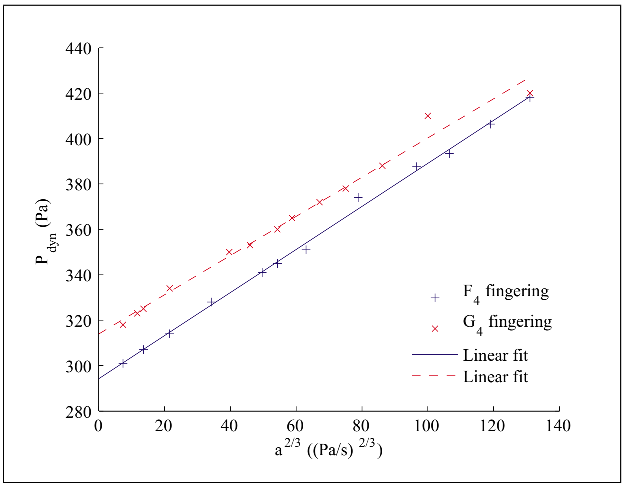

Figure 20. Time-domain simulations of linear increasing ramps of the blowing pressure, for both the F_4 fingering (+) and the G_4 fingering (x): representation of the dynamic regime change threshold $P_{dyn\ 1\rightarrow 2}$ with respect to the power 2/3 of the slope a. Solid and dashed lines represent linear fit of the data, which both present linear correlation coefficients with the data higher than 0.99.

through numerical continuation (see Figure 12 for the bifurcation diagram of the G_4 fingering), which supports the validity of the proposed modelling.

Moreover, the validity of the proposed modelling has also been checked in the case of the piecewise linear ramps of the blowing pressure studied in Section 3.3. For sake of clarity, both the details of calculations and the figure highlighting the good agreement beetwen simulation results and prediction of the model are provided in the appendix.

4.3. Case of experimental data

The experimental thresholds displayed in Figure 11 for the five fingerings studied are represented in Figure 21 with respect to $a^{2/3}$. Similarly to Figure 20, the different curves are correctly fitted by straight lines, with linear correlation coefficients between 0.88 and 0.99. The fact that these coefficients are, in some cases, lower than those of simulations can be explained by the presence of noise and of small fluctuations of the mouth pressure during the experiment, which sometimes prevents a threshold detection as accurate and systematic as in the case of numerical results. However, the good agreement of the experimental results with Equation (12) also allows to validate the proposed phenomenological modelling of regime change.

4.4. Influence of the regime resulting from the regime change

In the case of time-domain simulations, for the G_4 fingering, starting from the second register and achieving linear decreasing ramps of $P_m(t)$ leads to a particular behaviour. As shown in Figure 22, P_{dyn} does not appear, at least in a first stage, to be proportional to the power 2/3 of the slope. However, this case is particular in the sense that different oscillation regimes are reached, depending on the slope a

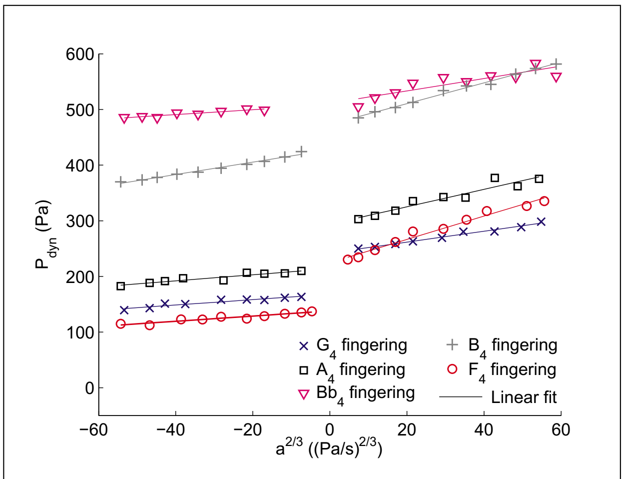

Figure 21. Same data as in Figure 11: representation of the dynamic thresholds $P_{dyn\ 1\to2}$ and $P_{dyn\ 2\to1}$, for five fingerings of an alto recorder played by an artificial mouth, with respect to the power 2/3 of the slope a of linear ramps of the blowing pressure. Solid lines represent linear fit of the data. Data present linear correlation coefficients between 0.88 and 0.99.

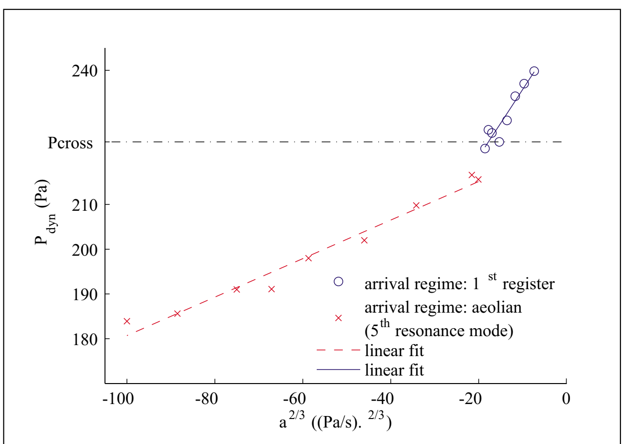

Figure 22. Time-domain simulations of linear decreasing ramps of the blowing pressure, for the G_4 fingering: representation of the dynamic regime change threshold $P_{dyn\ 2\to1}$ with respect to the power 2/3 of the slope a. Circles and crosses represent transitions from the second register to the first register and to an aeolian regime, respectively. Solid and dashed lines represent linear fit of the data, which present linear correlation coefficients of 0.98 and 0.95, respectively. The dashed line indicates the pressure at which the Floquet exponents of the starting regime cross in Figure 23.

of the ramp. Thereby, as highlighted with circles in Figure 22, low values of the slope ($|a| < 20$ Pa/s) lead to a transition from the second to the first register, whereas higher values of the slope lead to a transition from the second register to an aeolian regime, as represented with crosses in Figure 22. In recorder-like instruments, aeolian regimes correspond to particular sounds, occuring at low values of the blowing pressure, and originating from the coupling between a mode of the resonator (here the 5^{th}) and an hydrodynamic mode of the jet of order higher than 1 [7, 53, 4].

As highlighted in the same figure, considering the two different transitions separately allows to find, as previously, the linear dependence between P_{dyn} and $a^{2/3}$. Indeed, linear correlation coefficients of 0.98 for $|a| < 20$ Pa/s, and of 0.95 for $|a| > 20$ Pa/s are found. Since the corresponding slope is the inverse of $2/3\alpha$ to the power 2/3 (see Equation 12), such results suggest that α does not only depend on the fingering, but also on the oscillation regimes involved in the transition.

The study of the Floquet exponents ρ_m of the system supports this hypothesis. The Floquet exponents, computed for the system linearised around one of its periodic solutions, allow to estimate the (local) stability properties of the considered periodic solution [54, 37]. More precisely, they provide information on whether a small perturbation superimposed on the solution will be amplified or attenuated with time. If all the Floquet exponents have negative real parts, any perturbation will be attenuated with time, and the considered solution is thus stable. Conversely, if at least one of the Floquet exponents has a positive real part, any perturbation will be amplified in the "direction" of the phase space corresponding to the eigenvector associated to this exponent, and the solution is thus unstable.

The real part of the Floquet exponents of the considered system, linearised around the periodic solution corresponding to the second register (*i.e.* to the "starting" regime of the decreasing blowing pressure ramps considered here), are represented in Figure 23 with respect to the blowing pressure P_m. It highlights that the second register is stable for all values of P_m between 300 Pa and 259 Pa. A first Floquet exponent introduces an instability at $P_m = 259$ Pa, wich corresponds to the destabilisation of the second register (see Figure 12). As highlighted in [9], such a destabilisation, corresponding to a bifurcation of the second register, causes the regime change. This point is thus the static threshold $P_{stat\ 2\to1}$, already highlighted in Figure 12. A second Floquet exponent reaches a positive real part at $P_m = 229$ Pa. Moreover, the real part of the latest exponent becomes higher than the first one for $P_m < P_{cross}$, with $P_{cross} = 224$ Pa.

Comparison between results presented in Figures 22 and 23 suggests that the *arrival* regime resulting from a regime change is driven by the highest Floquet exponent (in terms of real part) of the *starting* regime. Indeed, until the regime change threshold P_{dyn} remains higher than the pressure P_{cross} at which the Floquet exponents intersect, the "first" Floquet exponent (represented in blue dashed line in Figure 23) is the highest one (in terms of real parts), and a transition to the first register is observed. Increasing the slope a of the blowing pressure $P_m(t)$ induces a shift of P_{dyn}, which then becomes lower than P_{cross}. At P_{dyn}, the "second" Floquet exponent, represented in black dashed line in Figure 23, is thus higher (in terms of real part) than the "first" Floquet exponent represented in blue solid line. In such a case, the regime change leads to the aeolian regime.

This interpretation seems furthermore to be consistent with the slope change observed in Figure 22 and with the physical meaning of the real part of the Floquet exponents. Indeed, as the value of the real part of a Floquet exponent is related to the amplification of a perturbation with time, a high value of $\Re(\rho_m)$ should correspond to a small duration $\hat{t}_{dyn}$ of the regime change, whereas a small value of $\Re(\rho_m)$ should correspond to a high value of $\hat{t}_{dyn}$. Therefore, by analogy with Equations (9) and (10), coefficient α can be related to the evolution of $\Re(\rho_m)$ with respect to P_m. Thereby, a faster evolution of $\Re(\rho_m)$ with respect to ΔP should correspond to a higher value of α. Due to Equation (12), valid for linear ramps of $P_m(t)$, it finally corresponds to a smaller rate of change of the straight line linking P_{dyn} and $a^{2/3}$. This property is here verified by the comparison between Figures 22 and 23: the real part of the "second" floquet exponent (in thick black dashed line in Figure 23), related to a regime change to the aeolian regime, presents a bigger slope (with respect to $\Delta P = P_m - P_{stat}$) than the floquet exponent inducing a transition to the first register (in solid blue line in Figure 23). In the same way, the rate of change of straight line related in Figure 22 to the regime change toward the aeolian regime (dashed line) is smaller than that of the straight line related to the transition from the second to the first register (in solid line).

Surprisingly enough, these results thus highlight that bifurcation diagrams and associated Floquet stability analysis provide valuable information in the dynamic case, despite the fact that they involve the static bifurcation theory and a linearisation of the studied system around the "starting" periodic solution. In the dynamic case, they remain instructive on the following characteristics:

- the arrival regime resulting from the regime change,
- a qualitative indication on both the duration of the regime change and the evolution of P_{dyn} with respect to the slope a of $P_m(t)$, through an estimation of the parameter α,
- as highlighted in the previous section, the evolution of the oscillation amplitude and frequency with respect to the mouth pressure, even after the static threshold has been crossed.

5. Conclusion

Compared with the artificial mouth, the experienced recorder player is observed to shift significantly the regime change thresholds, and thus to enlarge the hysteresis. Less difference is observed between the non musician and the artificial mouth. The experimental and numerical results show that once the steady threshold has been reached, the regime change thresholds (and thus the hysteresis) depend of the rate of increase or decrease of the blowing pressure. Modification of the dynamics of the blowing pressure can thus allow a player to avoid or to favor a given oscillation regime, and thereby to select the note following a regime change.

The proposed phenomenological model of regime change predicts the dynamic regime change threshold from the temporal profile of the blowing pressure. Bifurcation diagrams and the associated Floquet stability analysis help explain the dynamic case.

Experimentally, the influence of the blowing pressure dynamics is not enough to explain the thresholds and hysteresis produced by the experienced player, probably because other playing parameters (such as the shape of the blowing pressure profile and the vocal tract) are involved.

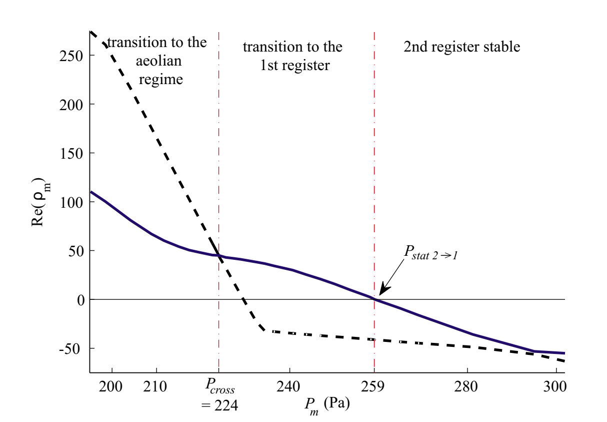

Figure 23. G_4 fingering: real parts of the Floquet exponents of the system linearised around the periodic solution corresponding to the second register, with respect to the blowing pressure P_m. Floquet exponents provide information on the stability properties of the considered regime.

Appendix: Validation of the phenomenological model of register change in the case of piecewise linear ramps of the blowing pressure

The validity of the proposed phenomenological model of register change has been tested, in Section 4.2, for the case of linear increasing and decreasing ramps of the mouth pressure. The case of piecewise linear ramps achievied experimentally and in time-domain simulation (see Section 3.3) is now examined, to determine if the model allows to predict the value of the dynamic regime change threshold.

According to the proposed model, the regime change occurs (and is observable) at time $\hat{t}_{dyn}$, at which $\zeta(\hat{t}_{dyn}) = \int_0^{\hat{t}_{dyn}} f(\Delta P)\,\mathrm{d}\hat{t} = 1$.

Contrary to the case of linear ramps, function $\Delta P(\hat{t})$ can no longer be written simply. Consequently, the first (linear) part of the pressure profile, with slope a_1, is first considered and the value of ζ reached at time $\hat{t}_{knee}$ (at which the slope break occurs) is computed through

$$\zeta(\hat{t}_{knee}) = \int_0^{\hat{t}_{knee}} f(\Delta P)\,\mathrm{d}\hat{t}. \tag{A1}$$

As demonstrated in Section 4.1, $f(\Delta P) = \alpha\sqrt{(\Delta P)}$. Moreover, on this first linear part of the pressure profile,

$\Delta P(\hat{t}) = a_1\hat{t}$. Equation A1 is thus rewritten as

$$\begin{aligned}\zeta(\hat{t}_{knee}) &= \int_0^{\hat{t}_{knee}} \alpha\sqrt{\Delta P}\,\mathrm{d}\hat{t}\\ &= \int_0^{\hat{t}_{knee}} \alpha\sqrt{a_1\hat{t}}\,\mathrm{d}\hat{t}\\ &= \alpha\sqrt{a_1}\int_0^{\hat{t}_{knee}} \sqrt{\hat{t}}\,\mathrm{d}\hat{t}\\ &= \frac{2}{3}\alpha\sqrt{a_1}\hat{t}_{knee}^{3/2}.\end{aligned} \tag{A2}$$

Taking into account the fact that $\hat{t}_{knee} = \Delta P_{knee}/a_1$, the following expression is finally obtained:

$$\zeta(\Delta P_{knee}) = \frac{2\alpha}{3a_1}\Delta P_{knee}^{3/2}. \tag{A3}$$

The second (linear) part of the mouth pressure profile is now considered, and the time required to reach the value $\zeta = 1$ is computed through

$$\int_{\hat{t}_{knee}}^{\hat{t}_{dyn}} f(\Delta P)\,\mathrm{d}\hat{t} = 1 - \zeta(\Delta P_{knee}). \tag{A4}$$

On this second linear part of the profile, the evolution of pressure with respect to time is written through $\Delta P(\hat{t}) = \Delta P_{knee} + a_2\hat{t}$. Substituting, as above, the expressions of $f(\Delta P)$ and $\Delta P(\hat{t})$ in Equation (A4) leads to

$$\int_{\hat{t}_{knee}}^{\hat{t}_{dyn}} \alpha\sqrt{a_2\hat{t} + \Delta P_{knee}}\,\mathrm{d}\hat{t} = 1 - \zeta(\Delta P_{knee}); \tag{A5}$$

$$\frac{2\alpha}{3a_2}\left\{\left[\Delta P_{knee} + a_2\left(\hat{t}_{dyn} - \hat{t}_{knee}\right)\right]^{3/2} - \Delta P_{knee}^{3/2}\right\} = 1 - \zeta(\Delta P_{knee}); \tag{A6}$$

$$\hat{t}_{dyn} = \frac{1}{a_2}\left[\frac{3a_2}{2\alpha}\left(1 - \zeta(\Delta P_{knee})\right) + \Delta P_{knee}^{3/2}\right]^{2/3} - \frac{\Delta P_{knee}}{a_2} + \hat{t}_{knee}. \tag{A7}$$

By knowing that $\hat{t}_{knee} = \Delta P_{knee}/a_1$ and substituting $\zeta(\Delta P_{knee})$ by its expression determined in Equation (A3), one obtains

$$\hat{t}_{dyn} = \frac{1}{a_2}\left\{\frac{3a_2}{2\alpha} - \Delta P_{knee}^{3/2}\left(1 - \frac{a_2}{a_1}\right)\right\}^{2/3} + \Delta P_{knee}\left(\frac{1}{a_1} - \frac{1}{a_2}\right). \tag{A8}$$

Knowing this expression of $\hat{t}_{dyn}$, the value of P_{corr}, defined in Section 4.1, can now be computed,

$$P_{corr} = \Delta P(\hat{t}_{dyn}) = \Delta P_{knee} + a_2(\hat{t}_{dyn} - \hat{t}_{knee}), \tag{A9}$$

$$P_{corr}^{3/2} = \frac{3a_2}{2\alpha} - \left(1 - \frac{a_2}{a_1}\right)\Delta P_{knee}^{3/2}. \tag{A10}$$

According to the proposed model, the dynamic regime change threshold power $3/2$ should thus be an affine function of ΔP_{knee} to the power $3/2$. To check the validity of the model, Figure A1 represents, for the same data presented in Figure 17, the value of P_{corr} to the power 3/2 with respect to the difference between the pressure P_{knee} at which the knee occurs and the static regime change threshold. It is recalled that these data correspond to time-domain simulations (G_4 fingering) of piecewise linear ramps of the blowing pressure, with $a_1 = 500$ Pa/s and $a_2 = 830$ Pa/s. As predicted by the model, a linear relation is observed between $P_{corr}^{3/2}$ and $\Delta P_{knee}^{3/2}$: the linear fit (highlighted in solid line) presents a correlation coefficient with the data higher than 0.99 (the corresponding p-value is less than 1^{-12}).

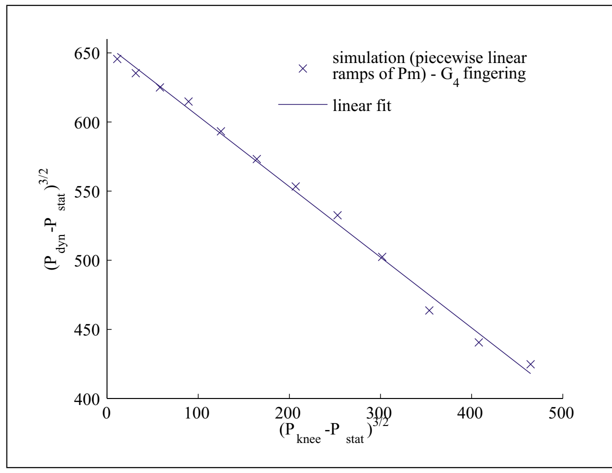

Figure A1. Time-domain simulations of increasing piecewise linear ramps of the blowing pressure ($a_1 = 500$ Pa/s and $a_2 = 830$ Pa/s), for the G_4 fingering. Representation of the difference between the dynamic regime change threshold and the static regime change threshold to the power 3/2, with respect to the power 3/2 of the difference between the pressure P_knee at which the slope break occurs and the static regime change threshold. The solid line represents linear fit of the data, which present a near correlation coefficient higher than 0.99.

Aknowledgment

The authors would like to thank Marine Sablonnière and Etienne Thoret for their participation in experiments.

References

[1] J. W. Coltman: Jet drive mechanisms in edge tones and organ pipes. Journal of the Acoustical Society of America **60** (1976) 725–733.

[2] Y. Sawada, S. Sakaba: On the transition between the sounding modes of a flute. The Journal of the Acoustical Society of America **67** (1980) 1790–1794.

[3] R. Auvray, B. Fabre, P. Y. Lagrée: Regime change and oscillation thresholds in recorder-like instruments. Journal of the Acoustical Society of America **131** (2012) 1574–1585.

[4] S. Terrien, C. Vergez, B. Fabre: Flute-like musical instruments: A toy model investigated through numerical continuation. Journal of sound and vibration **332** (2013) 3833–3848.

[5] C. Ségoufin, B. Fabre, L. de Lacombe: Experimental investigation of the flue channel geometry influence on edge-tone oscillations. Acta Acustica united with Acustica **90** (Sep. 2004) 966–975.

[6] C. Ségoufin, B. Fabre, M. P. Verge, A. Hirschberg, A. P. J. Wijnands: Experimental study of the influence of the mouth geometry on sound production in a recorder-like instrument: Windway length and chamfers. Acta Acustica united with Acustica **86** (2000) 649–661.

[7] N. H. Fletcher: Sound production by organ flue pipes. Journal of the Acoustical Society of America **60** (1976) 926–936.

[8] J. W. Coltman: Jet offset, harmonic content, and warble in the flute. Journal of the Acoustical Society of America **120** (2006) 2312–2319.

[9] S. Terrien, C. Vergez, B. Fabre, D. Barton: Calculation of the steady-state oscillations of a flute model using the orthogonal collocation method. Acta Acustica united with Acustica **100** (2014) 690–704.

[10] D. Ferrand, C. Vergez, B. Fabre, F. Blanc: High-precision regulation of a pressure controlled artificial mouth: The case of recorder-like musical instruments. Acta Acustica united with Acustica **96** (July 2010) 701–712.

[11] J. W. Coltman: Time-domain simulation of the flute. Journal of the Acoustical Society of America **92** (1992) 69–73.

[12] N. H. Fletcher: Acoustical correlates of flute performance technique. The Journal of the Acoustical Society of America **57** (1975) 233–237.

[13] F. Garcia, L. Vinceslas, J. Tubau, E. Maestre: Acquisition and study of blowing pressure profiles in recorder playing. Proceedings of the International Conference on New interfaces for Musical Expression, Oslo, Norway, 2011.

[14] P. de la Cuadra, B. Fabre, N. Montgermont, L. de Ryck: Analysis of flute control parameters: A comparison between a novice and an experienced flautist. Forum Acusticum, Budapest, 2005.

[15] B. Bergeot, A. Almeida, C. Vergez, B. Gazengel: Prediction of the dynamic oscillation threshold in a clarinet model with a linearly increasing blowing pressure. Nonlinear Dynamics **73** (2013) 521–534.

[16] B. Bergeot, A. Almeida, B. Gazengel, C. Vergez, D. Ferrand: Response of an artificially blown clarinet to different blowing pressure profiles. The Journal of the Acoustical Society of America **135** (2014) 479–490.

[17] E. Benoît: Dynamic bifurcations: proceedings of a conference held in luminy, france, march 5-10, 1990. Springer, 1991.

[18] D. H. Lyons: Resonance frequencies of the recorder (english flute). The Journal of the Acoustical Society of America **70** (1981) 1239–1247.

[19] H. von Helmholtz: On the sensation of tones. Dover New York, 1954.

[20] M. E. McIntyre, R. T. Schumacher, J. Woodhouse: On the oscillations of musical instruments. Journal of the Acoustical Society of America **74** (1983) 1325–1345.

[21] B. Fabre, A. Hirschberg: Physical modeling of flue instruments: A review of lumped models. Acta Acustica united with Acustica **86** (2000) 599–610.

[22] J. W. S. Rayleigh: The theory of sound second edition. New York, Dover, 1894.

[23] P. de la Cuadra, C. Vergez, B. Fabre: Visualization and analysis of jet oscillation under transverse acoustic perturbation. Journal of Flow Visualization and Image Processing **14** (2007) 355–374.

[24] A. Nolle: Sinuous instability of a planar jet: propagation parameters and acoustic excitation. Journal of the Acoustical Society of America **103** (1998) 3690–3705.

[25] M. P. Verge, R. Caussé, B. Fabre, A. Hirschberg, A. P. J. Wijnands, A. van Steenbergen: Jet oscillations and jet drive in recorder-like instruments. Acta Acustica united with Acustica **2** (1994) 403–419.

[26] M. P. Verge, A. Hirschberg, R. Caussé: Sound production in recorder-like instruments. ii. a simulation model. Journal of the Acoustical Society of America **101** 2925–2939.

[27] P. de la Cuadra: The sound of oscillating air jets: Physics, modeling and simulation in flute-like instruments. Dissertation. Stanford University, 2005.

[28] A. Chaigne, J. Kergomard: Acoustique des instruments de musique (acoustics of musical instruments). Belin (Echelles), 2008.

[29] B. Fabre, A. Hirschberg, A. P. J. Wijnands: Vortex shedding in steady oscillation of a flue organ pipe. Acta Acustica united with Acustica **82(6)** (1996) 863–877.

[30] A. Lefebvre: The wind instrument acoustic toolkit. http://www.music.mcgill.ca/caml/doku.php?id=wiat:wiat. Accessed: 2014-03-18.

[31] P. Bogacki, L. F. Shampine: A 3(2) pair of Runge-Kutta formulas. Applied Mathematics Letter **2** (1989) 321–325.

[32] K. Engelborghs, T. Luzyanina, K. J. In't Hout, D. Roose: Collocation methods for the computation of periodic solutions of delay differential equations. SIAM Journal on Scientific Computing **22** (2000) 1593–1609.

[33] B. Krauskopf, H. M. Osinga, J. Galan-Vioque: Numerical continuation methods for dynamical systems. Springer, 2007.

[34] E. J. Doedel: Lecture notes on numerical analysis of nonlinear equations. – In: Numerical Continuation Methods for dynamical systems. Springer, 2007, 1–49.

[35] D. Barton, B. Krauskopf, R. E. Wilson: Collocation schemes for periodic solutions of neutral delay differential equations. Journal of Difference Equations and Applications **12** (2006) 1087–1101.

[36] D. Barton, B. Krauskopf, R. E. Wilson: Bifurcation analysis tools for neutral delay equations: a case study. 6th IFAC conference on Time-Delay Systems, 2006.

[37] A. H. Nayfeh, B. Balachandran: Applied nonlinear dynamics. Wiley, 1995.

[38] K. Engelborghs: DDE Biftool: a Matlab package for bifurcation analysis of delay differential equations. Tech. Rept. Katholieke Universiteit Leuven, 2000.

[39] K. Engelborghs, T. Luzyanina, D. Roose: Numerical bifurcation analysis of delay differential equations using DDE-Biftool. ACM Transactions on Mathematical Software **28** (2002) 1–21.

[40] S. Karkar, C. Vergez, B. Cochelin: Oscillation threshold of a clarinet model: a numerical continuation approach. Journal of the Acoustical Society of America **131** (2012) 698–707.

[41] S. Karkar, C. Vergez, B. Cochelin: Toward the systematic investigation of periodic solutions in single reed woodwind instruments. Proceedings of the 20th International Symposium on Music Acoustics, Sydney, Australia, Aug. 2010.

[42] A. de Cheveigné, H. Kawahara: Yin, a fundamental frequency estimator for speech and music. The Journal of the Acoustical Society of America **111** (2002) 1917–1930.

[43] J. P. Dalmont, B. Gazengel, J. Gilbert, J. Kergomard: Some aspects of tuning and clean intonation in reed instruments. Applied Acoustics **46** (1995) 19–60.

[44] S. Terrien, C. Vergez, P. de la Cuadra, B. Fabre: Is the jet-drive flute model able to produce modulated sounds like flautas de chinos ? Proceedings of Stockholm Music Acoustics Conference, Stockholm, Sweden, 2013.

[45] S. Terrien, R. Auvray, B. Fabre, P. Y. Lagrée, C. Vergez: Numerical resolution of a physical model of flute-like instruments: comparison between different approaches. Proceedings of Acoustics 2012, Nantes, France, 2012.

[46] R. Auvray, B. Fabre, P. Y. Lagrée, S. Terrien, C. Vergez: Influence of the fluctuations of the control pressure on the sound production in flute-like instruments. Proceedings of Acoustics 2012, Nantes, France, 2012.

[47] B. Fabre, F. Guillard, M. Solomon, F. Blanc, V. Sidorenkov: Structuring music in recorder playing: a hydrodynamical analysis of blowing control parameters. Proceedings of the International Symposium in Music and Acoustics, 2010.

[48] J. W. Coltman: Mouth resonance effects in the flute. The Journal of the Acoustical Society of America **54** (1973) 417–420.

[49] V. Fréour, G. P. Scavone: Vocal-tract influence in trombone performance. Proc. Int. Symp. Music Acoustics, Sydney & Katoomba, 2010.

[50] G. P. Scavone, A. Lefebvre, A. R. da Silva: Measurement of vocal-tract influence during saxophone performance. The Journal of the Acoustical Society of America **123** (2008) 2391–2400.

[51] J. M. Chen, J. Smith, J. Wolfe: Pitch bending and glissandi on the clarinet: roles of the vocal tract and partial tone hole closure. The Journal of the Acoustical Society of America **126** (2009) 1511–1520.

[52] P. Guillemain, C. Vergez, D. Ferrand, A. Farcy: An instrumented saxophone mouthpiece and its use to understand how an experienced musician plays. Acta Acustica united with Acustica **96** (2010) 622–634.

[53] M. Meissner: Aerodynamically excited acoustic oscillations in cavity resonator exposed to an air jet. Acta Acustica united with Acustica **88** (2001) 170–180.

[54] G. Floquet: Sur les equations differentielles lineaires. Ann. ENS [2] **12** (1883) 47–88.